GDCh Research Article Angewandte International Edition Chemie www.angewandte.org

How to cite: *Angew. Chem. Int. Ed.* **2024**, *63*, e202409322
doi.org/10.1002/anie.202409322

Zinc Metal Batteries

Interfacial Engineering of Polymer Membranes with Intrinsic Microporosity for Dendrite-Free Zinc Metal Batteries

Rui Tan[+], Hongzhen He[+], Anqi Wang, Toby Wong, Yilin Yang, Sunshine Iguodala, Chunchun Ye, Dezhi Liu, Zhiyu Fan, Mate Furedi, Guanjie He, Stefan Guldin, Dan J. L. Brett, Neil B. McKeown, and Qilei Song**

Abstract: Metallic zinc has emerged as a promising anode material for high-energy battery systems due to its high theoretical capacity (820 $mAh\,g^{-1}$), low redox potential for two-electron reactions, cost-effectiveness and inherent safety. However, current zinc metal batteries face challenges in low coulombic efficiency and limited longevity due to uncontrollable dendrite growth, the corrosive hydrogen evolution reaction (HER) and decomposition of the aqueous $ZnSO_4$ electrolyte. Here, we report an interfacial-engineering approach to mitigate dendrite growth and reduce corrosive reactions through the design of ultrathin selective membranes coated on the zinc anodes. The submicron-thick membranes derived from polymers of intrinsic microporosity (PIMs), featuring pores with tunable interconnectivity, facilitate regulated transport of Zn^{2+}-ions, thereby promoting a uniform plating/stripping process. Benefiting from the protection by PIM membranes, zinc symmetric cells deliver a stable cycling performance over 1500 h at 1 mA/cm^2 with a capacity of 0.5 mAh while full cells with $NaMnO_2$ cathode operate stably at 1 $A\,g^{-1}$ over 300 cycles without capacity decay. Our work represents a new strategy of preparing multifunctional membranes that can advance the development of safe and stable zinc metal batteries.

Introduction

The widespread adoption of lithium-ion batteries faces challenges due to the flammability of organic electrolyte and the cost of lithium resources, necessitating the development of safer and more economical alternatives.[1] Aqueous zinc metal batteries (ZMBs) are increasingly recognized among various metal-ion battery systems for their affordability and the incorporation of non-flammable and highly conductive aqueous electrolytes. Zinc metal also provides a promising solution for achieving efficient and high-energy storage due to its high gravimetric capacity, i.e., 820 $mAh\,g^{-1}$, and two-electron redox reactions at −0.762 V versus the standard hydrogen electrode (SHE).[2] However, the further advance of ZMBs is impeded by the uncontrollable dendrite problem and side reactions at the zinc surface, e.g., Hydrogen Evolution Reaction (HER) and zinc hydroxy sulphate (ZHS) based corrosive reactions (Figure 1a), leading to poor coulombic efficiency and short service time.[3] The generation of inert by-products and H_2 unexpectedly lead to non-homogenised Zn^{2+}-ion flux and exacerbate dendrite growth. Consequently, there is a critical need to develop durable strategies that can address the above-mentioned problems.[4]

Theoretically, the reactive surface of Zn anodes is where parasitic water decomposition inevitably occurs, leading to a dramatic decrease in local pH, which roughens surface morphology and causes heterogeneous deposition of Zn^{2+}-ions.[2b] Notably, the desolvation of Zn^{2+}-ions can release active water molecules within the electric double layer and further trigger the passivation reactions between the aqueous electrolyte and Zn metal. This results in the formation of zinc hydroxy sulphates that impede the zinc

[*] Dr. R. Tan,[+] Dr. A. Wang, Dr. T. Wong, Y. Yang, S. Iguodala, Dr. D. Liu, Z. Fan, Dr. Q. Song
Department of Chemical Engineering, Imperial College London, London SW7 2AZ, UK
E-mail: rui.tan@swansea.ac.uk
q.song@imperial.ac.uk

Dr. R. Tan[+]
Department of Chemical Engineering, Swansea University, Swansea SA1 8EN, UK
E-mail: rui.tan@swansea.ac.uk

H. He,[+] M. Furedi, Prof. S. Guldin, Prof. D. J. L. Brett
Department of Chemical Engineering, University College London, London, WC1E 7JE, UK

Dr. C. Ye, Prof. N. B. McKeown
EaStChem School of Chemistry, University of Edinburgh, Edinburgh, EH9 3FJ, UK

Dr. G. He
Department of Chemistry, University College London, London, WC1E 7JE, UK

[+] These authors contributed equally.

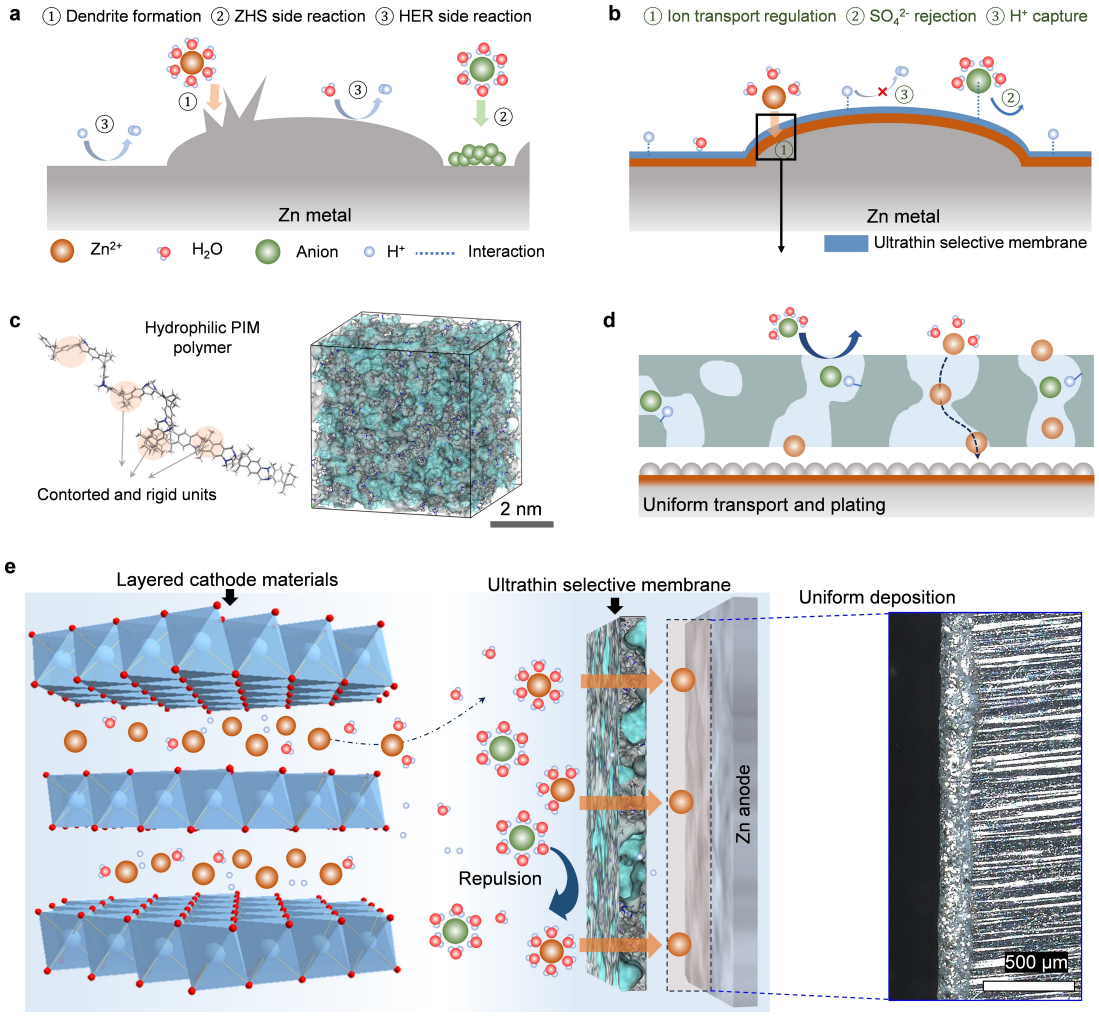

Figure 1. Design concept of selective and protective membrane coating on zinc anodes. **a**. Schematic illustration of dendrite and side-reaction challenges involved in systems with bare zinc. **b**. Proposed strategy of designing protective membranes for regulating ion transport and mitigating side reactions, HER and formation of ZHS byproducts. **c**. A polymer chain and a modelling cell of hydrophilic PIMs. **d**. Working principle of the selective protective ultrathin membranes and the interaction between ions and PIM structures. **e**, Diagram illustrating the working principles of a full Zn metal battery cell with layered cathode materials and Zn anode protected by the selective PIM membrane coating.

platting/stripping process and increase cycling polarization. Regulating the transport of Zn^{2+}-ions and immobilization of other species, i.e., water, proton and large anionic species, is one effective approach to solve the dendritic problem and avoid the side reactions.[5] Accordingly, various solutions have been proposed, such as the design of electrolyte additives,[6] modification of zinc deposition substrates,[7] functionalization of separator membranes and cathode coating strategies.[8] The surface protection of Zn anodes is a straightforward and efficient method for solving the passivation and corrosion problems and enabling uniform stripping/plating of metal ions, and enhancing the battery performance of ZMBs.[5a,6a,9] A variety of surface artificial protective layers have been developed to regulate the ion transport via the constructed pore channels or introduce nucleation barriers to guide the Zn deposition protection, such as metal oxides/sulfides (e.g., MoS_2),[10] polyelectrolytes (e.g., polyamide, polyacrylic acid, carboxymethyl cellulose, poly(vinyl butyral)),[5a,11] carbon black and graphene materials.[12] However, the ion transport channels in these materials are still poorly defined, leading to non-uniform transport Zn^{2+}-ions and protons, and consequently challenges with dendrite, passivation and HER corrosion reactions.[12a] The resulting redox-inactive layers with the thickness of more than several microns also sacrifice the output of volumetric energy.[12b,13] Metal–organic frameworks (MOFs) and covalent-organic frameworks (COFs) are promising for constructing defined pore channels and regulating Zn^{2+}-ion transport.[14] However, the construction of artificial protective layers using MOFs and COFs often involves sophisticated coating processes, and usually requires redox-inactive polymer binders to produce an integrated coating layer.[12a,14a] Given these challenges, it is desirable to develop multifunctional selective membranes that enhance overall battery performance through simple processing techniques.

Polymers of intrinsic microporosity (PIMs) represent a new class of polymer materials with highly interconnected micropores (size less than 2 nm according to IUPAC),[15]

which have shown great promise as a new generation of membranes with selective and uniform ionic transport in electrochemical devices. The solution-processability and versatile functionality of PIMs are particularly intriguing, enabling the creation of submicron-thick membranes with a customized functional structure for fast and selective transport of target ions.[16] PIM membrane coated on lithium could effectively enable uniform transport of lithium ions, which effectively mitigates the growth of Li dendrites in organic solvents and consequently promising performance in lithium metal batteries.[17] However, there remain challenges to deploy PIMs for addressing the issues involved in aqueous ZMBs due to the limited types of hydrophilic PIMs available and the difficulty of selecting compatible PIM chemistries to solve passivation and corrosion reactions in aqueous energy systems. Among various PIM chemistries, hydrophilic Tröger's base PIMs (TB-PIMs) have been demonstrated as thin film composite membranes in aqueous redox flow batteries.[15,18] Unlike MOFs, COFs and polyelectrolytes, solution-processable TB-PIMs can be readily coated onto zinc foil as ultrathin protective layers without the need for binders or post-thermal treatment. In addition, protonation of Tröger's base could afford these PIMs the capacity to capture and conduct protons. For instance, protonated Tröger's base units exhibited the capacity to immobilize negatively charged species, such as $Fe(CN)_6^{4-}$-ions,[19] through electrostatic attraction, thereby demonstrating their potential utility in selective ion transport applications. Therefore, we anticipate that TB-PIMs are promising materials for the design of multifunctional selective membrane coating for zinc metal anodes.

In this work, we report the interfacial engineering of zinc metal anode by coating an ultrathin layer of PIM membranes that effectively mitigate the zinc dendrite growth and reduce corrosive reactions. These TB-PIM membranes possess highly interconnected ion channels that facilitate uniform metal ion stripping/plating and reduce the formation of metallic dendrites (Figure 1b–c). Importantly, protonated Tröger's base units act as sites for proton binding, and the resulting electrostatic attraction promotes the capture of anionic species, i.e., SO_4^{2-}, mitigating the impact of HER and side reactions involving SO_4^{2-}-ions (Figure 1d). Zinc symmetric cells coated with TB-PIM membranes deliver a low nucleation overpotential of ~22.0 mV and stable cycling performance over 1500 h at 1 mA/cm^2. Moreover, TB-PIM membrane coating layer can direct the preferential orientation of Zn deposition along the (002) crystal plane. Integrated with Zn anode and $NaMnO_2$ cathode in a full cell, TB-PIM membrane enabled the stable operation of over 300 cycles with no observable capacity decay at 1 A g^{-1}. TB-PIM membrane can also extend the lifespan of Zn||VS_2 full cells that operate stably for over 900 cycles with a high coulombic efficiency of above 99.9 % and a capacity retention of 70.1 %, which was much more stable compared to that of full cells without TB-PIM protective films (capacity retention of 4.0 % after 900 cycles). Our work introduces a new strategy of preparing multifunctional membranes that address several challenges simultaneously and thereby advances the development of stable and safe zinc metal batteries (Figure 1e).

Results and Discussion

To demonstrate our proposed strategy, two prototypical TB-PIM polymers were selected based on ethanoanthracene (PIM-EA-TB) and dimethylbiphenyl (DMBP-TB) structural components (Figure S1). Both polymers possess highly interconnected micropores with apparent Brunauer–Emmett–Teller (BET) surface areas of 830 and 385 m^2 g^{-1}, respectively, as determined by nitrogen adsorption. TB-PIM chloroform solutions with concentrations of 1.0 and 2.0 wt % were spin-coated onto bare zinc metals to produce surface-tailored zinc with ultrathin coating, namely PIM-EA-TB@Zinc and DMBP-TB@Zinc (Figure 2a). To investigate the fundamental relationships between the free volume and selective ion transport, PIM-EA-TB and DMBP-TB with varied mass ratios were blended to prepare a series of PIM films with varied porosity (Figure S2). The "built-in" hydrophilic TB units within TB-PIM coatings can hydrophilize the surface of zinc metal as evidenced by the reduced contact angles from 88.7° to 70.5° in a 2.0 M $ZnSO_4$ solution (Figure 2b and Figure S3), indicating the enhanced affinity towards aqueous electrolyte. The wettability of TB-PIM coatings is crucial for the formation of continuous transport channels for Zn^{2+}-ions at the interface between zinc metal and coating film.[20] Additionally, the TB-PIM films are capable of smoothing and homogenizing the rough zinc surface, characterised by numerous pits and protrusions (Figure 2c), which is important to enable an even electrical field so as to induce the uniform deposition of metal ions and mitigate dendrite growth. Atomic force microscopy (AFM) images revealed that a submicron-thick film, about 200 to 300 nm, was coated on the zinc metal surfaces (Figure 2d, 2g and S4). These coatings exhibited smooth surface topographies with a roughness (Rq) in the range of 0.20–0.26 nm and an average roughness (Ra) of 0.16–0.22 nm (Figure 2e and 2h; Table S1). Despite their ultrathin nature, the prepared coatings still presented high and uniform modulus of 1.7–4.0 GPa (Figure 2f and 2i). A tape peel test was conducted to prove the stable attachment of coating films (Figure S4). Compared to coating films derived from MOFs, COFs and polyelectrolytes, the solution-processability of PIMs enables the easy creation of homogeneous and durable ultrathin films without binders or thermal processing (Table S2).

To tailor the size and pore connectivity, we blended a high-porosity PIM-EA-TB and a low-porosity DMBP-TB and obtained smooth and uniform thin films without observable nanophase separation (Figure S5–6). The homogeneous mixing of the two polymers with varied porosity allows precise control over ion transport properties. Figure 3a shows the simulated polymer models to visualize the pore volume and pore size distribution for PIM-EA-TB, DMBP-TB and their blends ($EA_3|DMBP_1$, $EA_2|DMBP_3$ and $EA_1|DMBP_4$). Gas sorption tests showed a decrease in CO_2 adsorption capacity with increasing weight ratio of

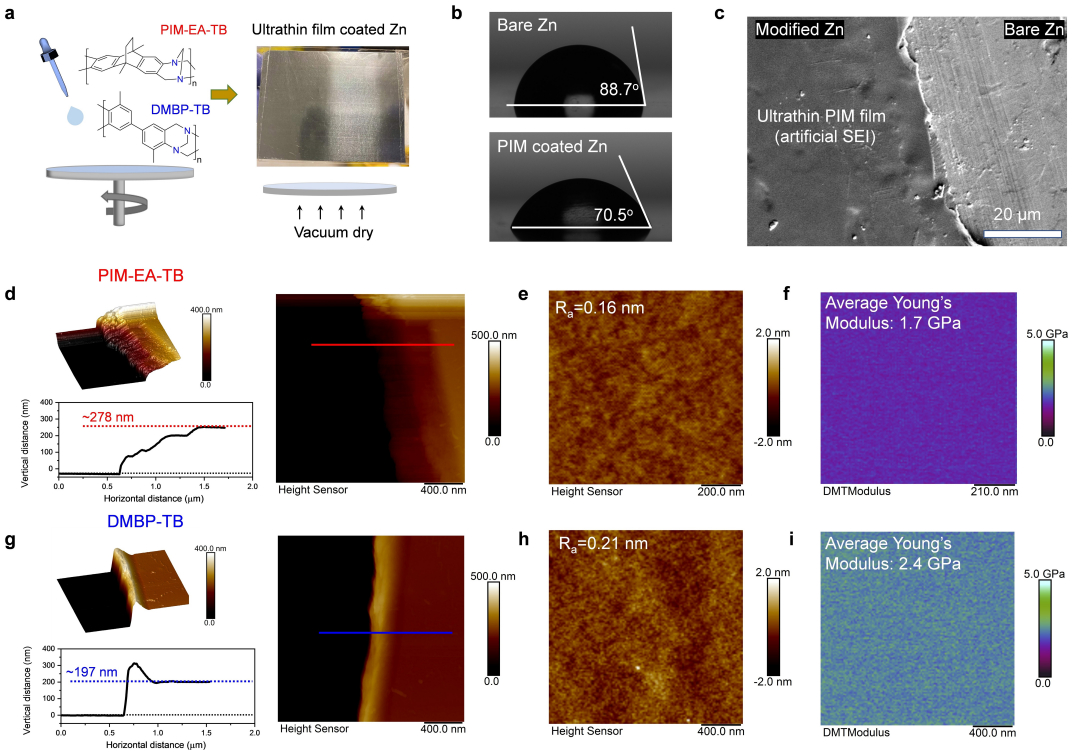

Figure 2. Selective coating film preparation and characterization. **a**. Schemes showing the preparation of polymer-coated Zn with PIM-EA-TB and DMBP-TB solutions by a spin-coating method onto Zn metal. **b**. Contact angle of bare Zn and TB-PIM coated Zn with a 2.0 M $ZnSO_4$ solution. **c**. Surface morphologies of PIM-EA-TB coated Zn and bare Zn. PIM-EA-TB coating: **d**. Thickness measurement using AFM. **e**. Surface roughness. **f**. Modulus mapping; DMBP-TB coating: **g**. Thickness measurement. **h**. Surface roughness. **i**. Modulus mapping.

DMBP-TB in the blends. The BET surface area determined by N_2 adsorption for PIM-EA-TB, $EA_3|DMBP_1$, $EA_2|DMBP_3$ and $EA_1|DMBP_4$ and DMBP-TB was 830, 692, 521, 455, 385 $m^2 g^{-1}$, respectively whilst all these polymers maintain a similar pore size distribution between 0.5–0.9 nm as derived from NLDFT model from CO_2 adsorption isotherms (Figure 3b–c). To explore the selective transport of ions within TB-PIM films in aqueous electrolyte, we employed ellipsometry tests and impedance and conductivity analysis. Ellipsometry tests suggested that the thicknesses of PIM film coated on zinc foils increased from 100 to 200 nm with the concentration of TB-PIM in chloroform solution varied from 1.0 to 2.0 wt % (Figure S7). Among them, PIM-EA-TB demonstrates the highest swelling ratio at a relative humidity of 1.0 owing to its abundant pore channels (Figure 3d; Table S3). The noticeable swelling confirm that PIM-EA-TB features the accessibility to aqueous electrolyte and enables the generation of a great number of pore channels, which is of importance for selective and fast ionic transport.

We measured the ionic transport resistance of thick TB-PIM films (~10 μm) in 2.0 M $ZnSO_4$ solutions from 20 to 80 °C by electrochemical impedance spectroscopy (Figure 3e–f). Compared with DMBP-TB and its blends, PIM-EA-TB displayed the lowest overall ohmic resistance of 2.41 Ω cm^2, suggesting limited hinderance for ion transport within the pore channels in PIM-EA-TB. The ionic conductivity of PIM-EA-TB is 0.22 mS/cm, which is much higher than those of $EA_2|DMBP_3$ and $EA_1|DMBP_4$ and DMBP-TB (0.10, 0.05 and 0.03 mS/cm, respectively). These TB-PIM membranes have comparable activation energies of 9.06–12.6 kJ mol^{-1} indicating that ions can smoothly migrate within the percolated pore channels while the overall conductivity is determined by the accessible pore channels (Figure 3g). The low ion transport resistance was further confirmed by resistance and polarization tests using Zn||Zn symmetric cells. PIM-EA-TB and DMBP-TB can both wet and homogenize the surface zinc metals to deliver low charge transfer resistances of 157.1 and 313.9 Ω, which are much lower than that of bare zinc metal (465.3 Ω, Figure S8). Overpotential, a critical electrochemical property, is used to assess the ion transport performance of coating films. Figure 3h shows a low nucleation potential for Zn^{2+}-ions through PIM-EA-TB (19.8 mV) and an overpotential ΔV of 46.8 mV, which is lower than other TB-PIM coatings. As the thickness of coating layer decreases, there is a corresponding reduction in the overpotential, as illustrated in Figure S9. Additionally, we compared the overpotential of our TB-PIM coating films against those of MOFs, COFs and polyelectrolytes, as listed in Table S2. TB-PIMs exhibit low overpotentials, performing comparably to other advanced microporous materials and significantly better than most polyelectrolytes (Figure S10).

Diffusion dialysis driven by salinity concentration and migration driven by the electrical field were carried out to investigate the selective transport of target Zn^{2+}-ions through TB-PIM membranes (Figure 3i–j). Interestingly, the

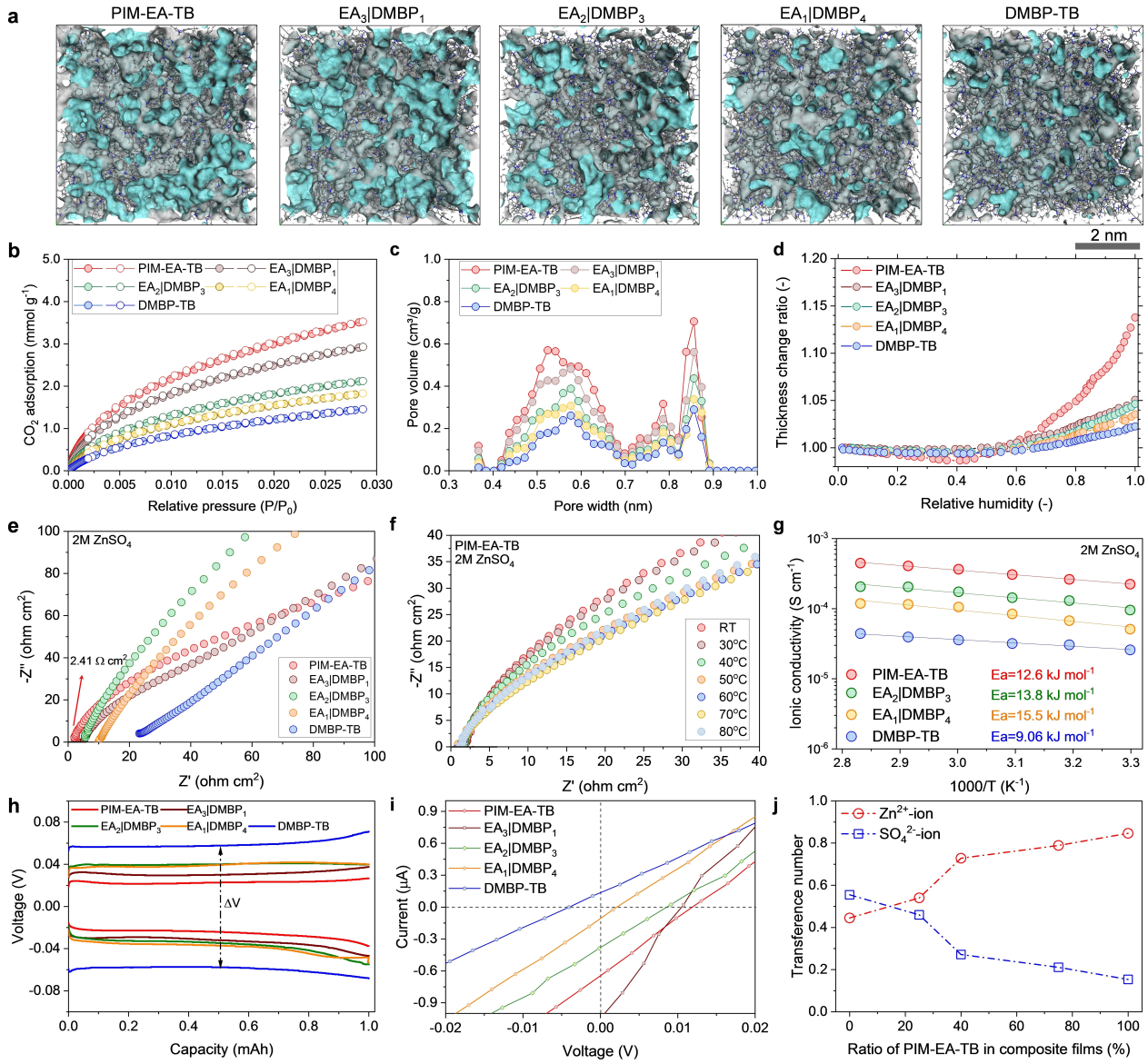

Figure 3. Micropore structures and selective ion transport. **a**. Simulated amorphous models for PIM-EA-TB, DMBP-TB and their blends: $EA_3|DMBP_1$, $EA_2|DMBP_3$ and $EA_1|DMBP_4$. Blue surface: the Connolly surface with a probe radius of 1.55 Å. **b**. CO_2 sorption isotherms. **c**. Pore size distribution derived from CO_2 sorption isotherms based on NLDFT models. **d**. Thickness change ratios at different relative humidity measured by ellipsometry. **e**. Areal specific resistance of TB-PIM membranes in 2.0 M $ZnSO_4$ solutions. **f**. Areal specific resistance of a PIM-EA-TB membrane in a 2.0 M $ZnSO_4$ solution at different temperatures. **g**. Arrhenius plots of TB-PIM membranes in 2.0 M $ZnSO_4$ solutions. **h**. Polarization curves of Zn||Zn symmetric cells at 1.0 mA cm^{-2} with a capacity of 1.0 mAh. **i**. Linear sweep voltammetry (LSV) of TB-PIMs at a scanning rate of 1 mV s^{-1} from −0.1 to 0.1 V. **j**. Transference number of Zn^{2+}-ions and SO_4^{2-}-ions with the increase of PIM-EA-TB in the blends. Transference numbers were derived from the LSV results.

zero-current–voltages increased from −5.0 to 10.0 mV with the concentration of PIM-EA-TB within the blends, showing the change from an anion-dominant to cation-dominant transport process. The transference number of cations was calculated using methodology reported in a previous report.[21] In the pristine $ZnSO_4$ solutions, the transference number of Zn^{2+}-ion is only 0.197.[22] With the ratio of PIM-EA-TB in the blend membranes increased from zero to 100 %, the Zn^{2+}-ion transference number increased from 0.445 to 0.846 while the transference number of SO_4^{2-}-ions decreased to 0.154 accordingly. The high porosity of PIM-EA-TB membrane allowed enhanced mobility of zinc ions due to hydrated zinc ions (4.3 Å). Tröger's base units in highly porous PIM-EA-TB ($pK_A \approx 4$)[19] can be readily protonated in the acidic $ZnSO_4$ solution (pH ≈ 3.6), which immobilizes the negatively charged sulphate anions due to electrostatic interactions. The strategy that uses protonated imine units to immobilize anions and creates selective transport channels for cations, has been employed in the design of highly conductive cation exchange membranes.[23] In this study, the interaction between anions and TB units is expected to decrease SO_4^{2-}-ion mobility, consequently

boosting Zn^{2+}-ion transference number (Figure 3j) and diminishing potential side reactions with zinc metal. Given that a portion of protons interacts with TB units, the concentration of remaining proton concentration is significantly lower than that of Zn^{2+}-ion by at least four orders of magnitude, making Zn^{2+}-ion the predominant migration ions.

We have systematically summarized the electrochemical details of PIM-EA-TB, DMBP-TB, and their blends in Table S4. It is clear that the BET surface area, indicative of polymer porosity and interconnected water channels, is crucial for determining selective ion transport performance. The PIM-EA-TB, with the highest BET surface area of 830 m^2/g, shows the most effective selective ion transport performance. To investigate the mechanism and demonstrate cell performance, we focused on PIM-EA-TB and DMBP-TB to elucidate the principles of ion transport. For cell demonstrations, we selected PIM-EA-TB, DMBP-TB, and a medium-porosity blend, $EA_2|DMBP_3$.

Selective Ion Transport Mechanisms

We anticipate that TB-PIM coating films can regulate the transport ions via two basic mechanisms, steric hinderance and Donnan effects. Steric-hinderance-based transport has been demonstrated in our previous reports.[15,18] To further investigate the ion regulation, we employed COMSOL Multiphysics to simulate the distribution of local current density and electric field at the interface between the anode and the electrolyte by adjusting the size of transport channels from 250 to 5 nm (Figure S11). As the decrease in channel sizes, the Zn^{2+}-ions are prone to permeate through coating films and accumulate in a 2D planar manner. Accordingly, we can deduce that TB-PIM coating films with smaller pore channels can effectively regulate and homogenize ion transport, which is also evidenced by the increased (002) X-ray diffraction analysis (XRD) peaks in Figure 4a–b. The activation energy of the plating of Zn^{2+}-ions is lower than that of reported bare Zinc and surface-modified Zn,[24] indicating that Zn^{2+}-ions tend to undergo the desolvation process while migrating through PIM-EA-TB coating films (Figure S12). Although PIM-EA-TB and DMBP-TB can regulate Zn^{2+}-ions to transport and growth in (002) planes, by-products (zinc hydroxy sulfate, marked as * in Figure 4a–b) can be barely observed in the Zn||Zn cells with PIM-EA-TB coatings, which suggests sulfate ions can be immobilized within the PIM-EA-TB film and isolated from redox active zinc metal, closely associated with the Donnan effects. A collective signal of –C–N–C– groups was clearly observed

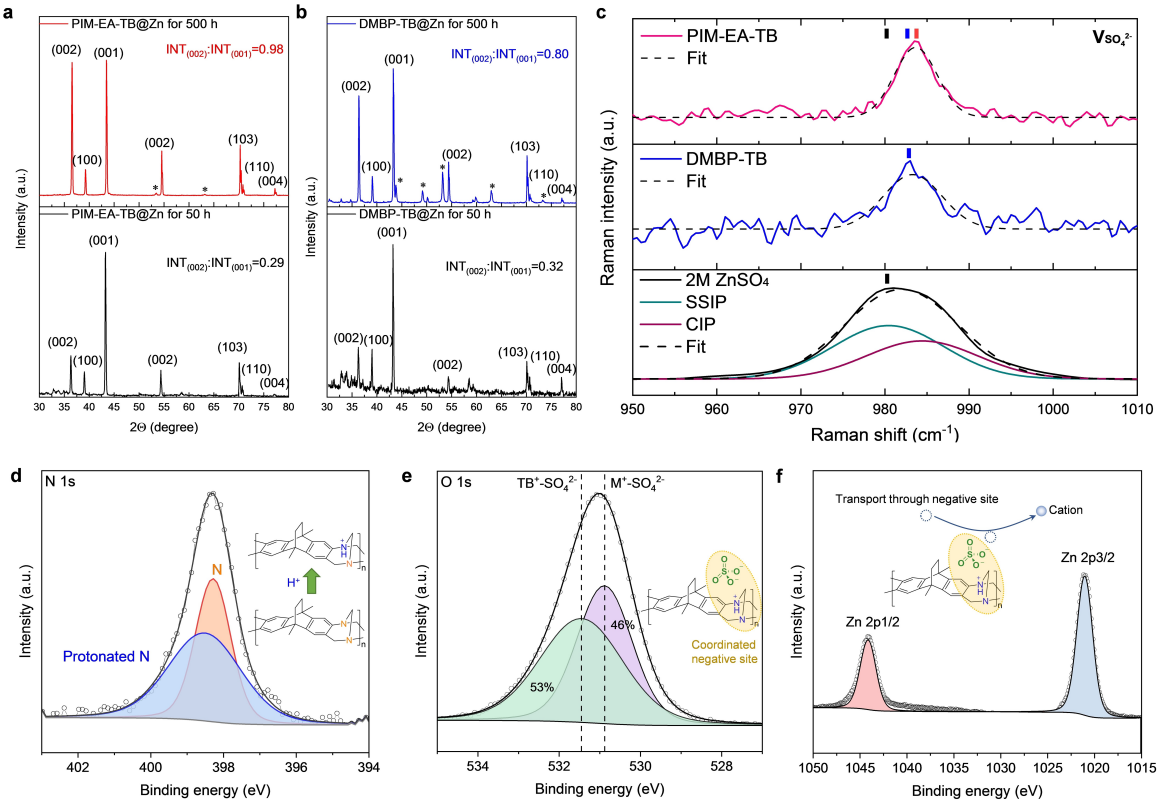

Figure 4. Selective ion transport mechanism. **a**. X-ray diffraction of PIM-EA-TB@Zn from the symmetrical cells that cycled for 50 and 500 hrs at 1.0 mA cm^{-2} with a capacity of 1.0 mAh. **b**. X-ray diffraction of DMBP-TB@Zn from the symmetrical cells that cycled for 50 and 500 hrs at 1.0 mA cm^{-2} with a capacity of 1.0 mAh. **c**. Raman spectra of $ZnSO_4$-pretreated PIM-EA-TB, $ZnSO_4$-pretreated DMBP-TB and pristine 2.0 M $ZnSO_4$ solution. XPS spectra of PIM-EA-TB@Zn treated by a 2.0 M $ZnSO_4$ solution: (**d**) N 1s, (**e**) O 1s, (**f**) Zn 2p1/2 and 2p3/2. Insets illustrate the interaction between ions and TB-PIM moieties.

in Fourier transform infrared (FT-IR) spectra (Figure S13), confirming the presence of TB-coating layer after 500 hrs of plating and stripping of Zn^{2+}-ions. This observation supports the durability of the TB-coating layer under prolonged electrochemical conditions.

To gain insights into the fundamental understanding of the ion-membrane interactions in TB-PIM membranes, we performed Raman Spectroscopy and X-ray photoelectron spectroscopy (XPS) study of membranes treated by a 2.0 M $ZnSO_4$ solution. Aqueous $ZnSO_4$ solution is a weak acidic solution (pH ≈ 3.6) that can protonate the Tröger's base to produce a change in the XPS spectrum[19] (Figure 4d). Protonation process was also observed by comparing the pristine free-standing membrane and $ZnSO_4$-treated membrane (Figure S14). Protons bind to Tröger's base units within polymers, allowing interactions with negatively charged sulfate ions. As shown in Figure 4c, this interaction alters the Zn^{2+} solvation structure, shifting from purely solvent-separated ion pairs (SSIP) to a combination of SSIP and contact ion pairs (CIP),[25] thereby affecting Zn^{2+} transport. The O 1s peak in the XPS can be deconvoluted into two distinct peaks (Figure 4e), one at a high binding energy representing the interaction between Zn^{2+} and SO_4^{2-} ions due to the strong inter-atomic effect; the other peak at a lower binding energy peak to the interaction between sulfate groups and protonated amine units (i.e., TB-units).[26] The interaction between negatively-charged sulfate groups and positively protonated amine units has also been observed in flow battery membranes.[27] This electrostatic attraction might immobilize sulfate ions and suppress the permeation of other free sulfate ions via Donnan effects, potentially enabling homogeneous and fast ion transport of Zn^{2+}-ions (Figure 4f). In comparison, from the deconvoluted O 1s peaks, DMBP-TB features less interacted sulfate ions (44.0 % in total) which might be responsible for the formation of noticeable sulfate-ion-based byproducts (Figure S15). Thus, TB-PIMs effectively utilize their microporous channels to regulate ion transport through size-exclusion mechanisms, while also employing protonated units to immobilize sulfate ions and enhance selective Zn^{2+}-ion transport via electrostatic interactions. This dual functionality plays a crucial role in stabilizing Zn^{2+}-ion stripping and plating while reducing HER and ZHS formation. Such multifunctionality is not typically achievable with other coating chemistries that typically adhere to a single working principle. For instance, MOFs and COFs depend almost exclusively on their well-defined micropores for ion regulation,[14] while polyelectrolytes without defined pores primarily employ electrostatic interactions to enhance ion transport.[5a,11]

The propagation and morphology of produced metallic dendrites were evaluated by a standard symmetric-cell protocol and an in situ optical microscope. Zn^{2+}-ions driven by an electrical field are stripped and plated on the surface of Zn metal in a 2.0 M $ZnSO_4$ aqueous solution at 1.0 mA cm^{-2} with a fixed capacity of 1 or 2 mAh. In consequence, both PIM-EA-TB and DMBP-TB membranes enabled high rate cycling performance at a capacity of 2 mAh from 1.0 to 20 mA cm^{-2}, then returning to 1.0 mA cm^{-2} without detectable short circuits and increased polarization overpotentials due to regulated ion flux and alleviated side reactions, i.e., HER and ZHS formation, (Figure 5a–b). Regarding long term evaluation, symmetric cells with Zn^{2+}-ions regulated by PIM-EA-TB membrane demonstrated a stable cycling life of 1500 hours without noticeable influence of dendritic issues whilst effectively conducting Zn^{2+}-ions and achieving a considerably low polarization potential of ~55 mV (Figure 5c). PIM-EA-TB@Zn disassembled from a cycled Zn||Zn symmetric cell presents a flat cross-sectional morphology without observable dendrites and protrusions (Figure S16). The DMBP-TB membrane delivers a reasonable 114 mV on initial cycles and also manages to sustain a stable cycling time of 1500 hour (Figure 5d). Blends with greater contribution of PIM-EA-TB over DMBP-TB provide coatings that reduce the overpotential whilst maintaining stable Zn^{2+}-ions stripping and plating process, which was evidenced by the cycling performance of Zn||Zn batteries using the $EA_2|DMBP_3$ coating film (Figure S17). The advantages of TB-PIM coatings can be underlined in the scenarios at high current densities, 10 and 20 mA cm^{-2}. Zn metal coated by TB-PIMs can maintain activity at 1000 cycles, equivalent to 200 hrs at 10 mA cm^{-2} with a stable stripping/plating plateau throughout cycling and consistently low overpotentials (Figure S17). At 20 mA cm^{-2}, TB-PIM coated Zn is capable of achieving 400 hours, confirming the effective protection of these selective membranes (Figure S18). In contrast, the control symmetric cell without the use of TB-PIM coatings exhibited a high overpotential of 163 mV and only survived for 261 hours, followed by an internal short circuit, likely caused by the penetration of accumulated zinc (namely dendrite) through separators (inset in Figure 5d).

To visualize the growth of dendrites and further validate the function of PIM membranes, we deployed in situ optical microscopy to image the cross-sectional morphology of Zn metal strips built in a homemade Zn||Zn symmetric cell. Round trip plating and stripping test was performed at 5 and 10 mAh cm^{-2} to induce fast growth of dendrites on the defective sites of Zn metal surface. With the non-regulated Zn^{2+}-ion transport and accompanying side reactions, rough and irregular Zn deposits with evident protrusions can immediately form on the bare Zn surface over only 10 cycles (Figure 5i–l). In contrast, TB-PIM coatings enabled flat and compact Zn plating with regular bulky sheets that correspond to the deposition of Zn^{2+}-ions following (002) plane (Figure 5e-h and S19). Importantly, even at a high current density of 200 mA cm^{-2}, PIM-EA-TB membrane can enable uniform transport and deposition of Zn^{2+}-ions (Figure S20). Furthermore, asymmetric Zn||Cu cells were established to evaluate the reversibility of Zn^{2+}-ion stripping and plating process through the surface membrane layers (Figure S21). All membranes derived from PIM-EA-TB, DMBP-TB and $EA_2|DMBP_3$ stabilize the stripping and plating process after 5–10 cycles and enable stable operation over subsequent cycles with high current efficiencies of ~100 %.

To further demonstrate the practical application of TB-PIM membranes in batteries, we employed three redox pairs, i.e., Zn||$NaMnO_2$, Zn||MnO_2 and Zn||VS_2, where

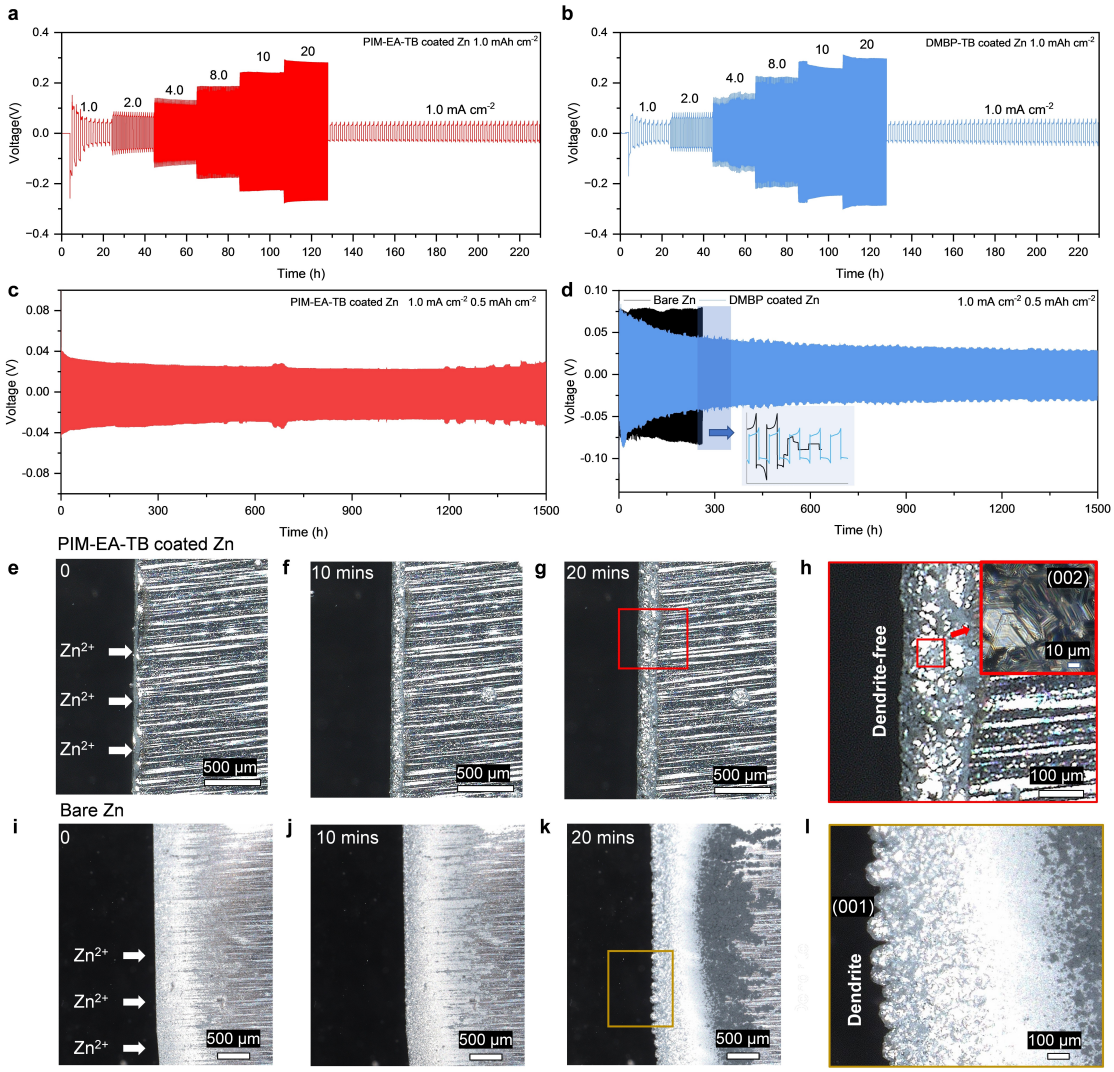

Figure 5. Performance of Zn||Zn symmetric cells and the growth of Zn dendrites. **a**. Rate performance of Zn||Zn symmetric cells using PIM-EA-TB coated Zn at currents of 1.0, 2.0, 4.0, 8.0, 10 and 20 mA cm^{-2} with a fixed capacity of 1.0 mAh cm^{-2}. **b**. Rate performance of Zn||Zn symmetric cells using DMBP-TB coated Zn at currents of 1.0, 2.0, 4.0, 8.0, 10 and 20 mA cm^{-2} with a fixed capacity of 1.0 mAh cm^{-2}. **c**. Long-term polarization tests of Zn||Zn symmetric cells using PIM-EA-TB@Zn at a current of 1.0 mA cm^{-2} with a fixed capacity of 0.5 mAh cm^{-2}. **d**. Long-term polarization tests of Zn||Zn symmetric cells using DMBP-TB@Zn at a current of 1.0 mA cm^{-2} with a fixed capacity of 0.5 mAh cm^{-2}. **e–h**. In situ optical microscopy images of Zn^{2+}-ion plating on PIM-EA-TB coated Zn metal at a current density of 10 mA cm^{-2} and up to 20 mins. **i–l**. In situ optical microscopy images of Zn^{2+}-ion plating on bare Zn metal at a current density of 10 mA cm^{-2} and up to 20 mins.

these chemistries are more sensitive to the variation of electrolyte conditions, such as pH, generated byproducts and dendrite influence. The cyclic voltammetry (CV) curves of the PIM-EA-TB@Zn||$NaMnO_2$, present distinct and typical redox peaks, which correlate to the reversible redox reaction between $NaMnO_2$ and NaMnOOH (Figure 6a). PIM-EA-TB@Zn||$NaMnO_2$ and DMBP-TB@Zn||$NaMnO_2$ cells demonstrated excellent performance at 0.2, 0.5, 1.0, 2.0, 3.0 A g^{-1} (Figure S22). The rapid electrochemical kinetics were evidenced by the stable and small charge transfer resistance for the PIM-EA-TB@Zn||$NaMnO_2$ cell that was cycled at given currents (Figure 6b). Furthermore, PIM-EA-TB@Zn||$NaMnO_2$, DMBP-TB@Zn||$NaMnO_2$ and $EATB_2$|$DMBP_3$@Zn||$NaMnO_2$ cells delivered a high specific capacity of 190 mAh g^{-1} at 1.0 A g^{-1} (Figure 6c). By using PIM-EA-TB membranes, dendrite and HER & side-reaction issues can be effectively mitigated, thereby enabling a stable cycling performance with a high capacity retention of 95 % and a high current efficiency of above 99.7 % over 300 cycles, outperforming the cycling life for bare Zn||$NaMnO_2$ cell (capacity retention: 43.9 % after 300 cycles; current efficiency: 99.5 %, Figure 6c and Figure S23). The electrochemical performance of Zn anodes coated with PIM-EA-TB, DMBP-TB, and $EATB_2$|$DMBP_3$, as summarized in Table S5, shows that all three membranes offer similar performance, indicating that moderate surface areas of PIMs are adequate for regulating ion transport. It is also worth noting that the low current densities typically used in ZMBs (0.1–5 A/g) may not effectively reveal the distinctions among these TB-PIM coatings.

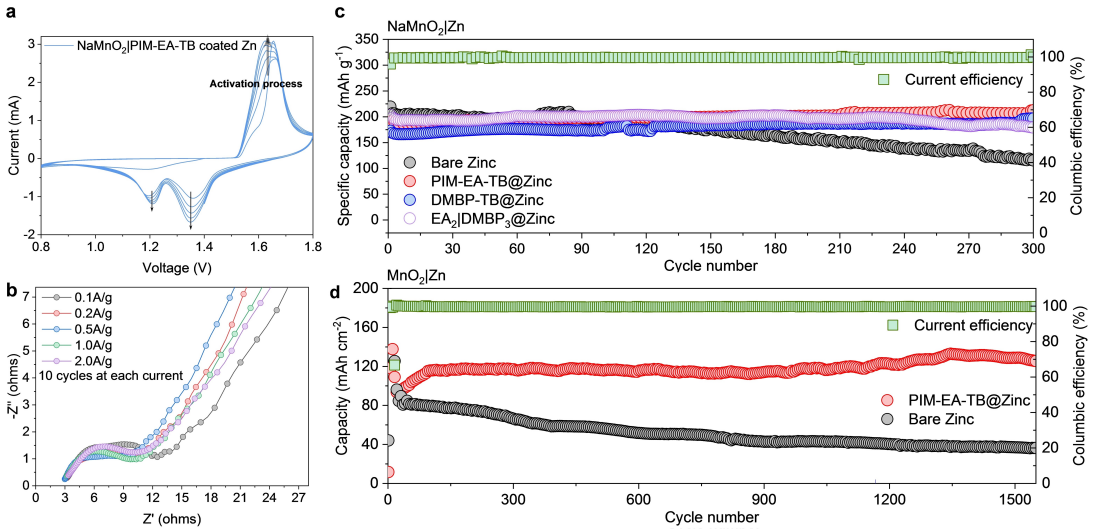

Figure 6. Full cell performance. **a**. Cyclic voltammetry of Zn||$NaMnO_2$ full cells with PIM-EA-TB coated Zn metal. **b**. Impedance of Zn||$NaMnO_2$ full cells with PIM-EA-TB@Zn cycled at varied current densities. **c**. Long-term cycling performance of Zn||$NaMnO_2$ full cells with PIM-EA-TB@Zn, DMBP-TB@Zn, $EATB_2$|$DMBP_3$@Zn and bare Zn. **d**. Long-term cycling performance of Zn||MnO_2 full cells with PIM-EA-TB@Zn and bare Zn.

Similarly improved duration of operation was also observed using PIM-EA-TB, DMBP-TB and $EATB_2$|$DMBP_3$ membranes in Zn||MnO_2 cells (Figure S24). For the long-term test, PIM-EA-TB, selected as the typical coating film, can stabilize the performance of the Zn||MnO_2 cell over 1500 cycles without apparent battery decay while the cell with the bare Zn showed rapid decay with the capacity retention of 57 % over 500 cycles (Figure 6d). Fast capacity decay was also observed for a cycling bare Zn||VS_2 cell where the severe HER and ZHS formation can directly deteriorate the structure of VS_2 and lead to irreversible electrochemical reactions. In comparison, our TB-PIM coatings can effectively protect the Zn metal and mitigate the dendrite growth and side reactions so as to deliver a high capacity retention of 70.1 % with an excellent coulombic efficiency above 99.9 % (Figure S25). Specifically, the TB-PIM enabled a capacity retention of 92.8 % after 200 cycles, much higher than that of the reported state-of-the-art Zn||VS_2 cell (~77.5 % capacity retention after 200 cycles).[28] Pouch cells assembled from PIM-EA-TB@Zn anode and MnO_2 cathode further demonstrated that the PIM coating contributes to stable battery cycling performance (Figure S26).

Conclusion

In summary, we reported a facile and effective strategy for zinc anode protection by ultra-thin selective hydrophilic PIM membranes and demonstrated stable operation of aqueous zinc metal batteries. In contrast to reported advanced coating chemistries (e.g., MOFs, COFs and polyelectrolytes), TB-PIM membranes with narrow pore channels and functional units offer unique multi-functions: (a) highly interconnected micropores provide abundant and uniform ion channels for homogeneous stripping/plating of metal ions, thereby eliminating the growth of Zn dendrites; (b) Tröger's base units are capable of anchoring protons partially via the protonation process and mitigate the HER that generally occurs on the zinc surface; (c) protonated Tröger's base units electrostatically attract the anionic species, i.e., SO_4^{2-}, and reduce the ZHS byproducts that are produced by the side reactions between SO_4^{2-} and Zn metal. Moreover, TB-PIM membrane coatings can enhance the wettability of the zinc metal surface and regulate the zinc ion transport, thereby reducing the overpotential for Zn^{2+}-ion transport and nucleation. As demonstrated in Zn||Zn symmetric cells, the PIM-EA-TB membrane achieved a remarkably low nucleation overpotential of ~20 mV and long-term performance for over 1500 h at 1 mA cm^{-2} without any observed influence from metallic dendrites. The elimination of dendrite growth was strongly evidenced by in situ optical microscopy at a high current density of 20 mA cm^{-2}. TB-PIM coatings enhanced the cycling performance of Zn||$NaMnO_2$, Zn||MnO_2 and Zn||VS_2 full cells, which exhibited long cycling durability with a high current efficiency (above 99.9 %). Our work represents a new strategy of preparing multi-functional selective and protective membranes that address multiple challenges and advance the development of stable and safe zinc metal batteries.

Experimental Section

Detailed Experimental Procedures and data are provided in the Supporting Information.

Author Contributions

Q.S. and R.T. conceived and designed the project. R.T. and H.Z.H. carried out most of the experiments, including

interfacial film fabrication, characterizations and battery tests. C.Y. and Z.Y.F. synthesized polymers. S.I. performed the molecular modelling. T.W. contributed to the NMR tests. Y.L.Y., contributed to the COMSOL simulation. M.F. and S.G. helped with the ellipsometry measurements. D.Z.L. helped with the characterization. C.J.L., G.H. and D. J.L.B. offered suggestions to this project. Q.S., R.T., and H.Z.H. wrote the manuscript with contributions from all authors. All authors discussed the results and commented on the manuscript at all stages.

Acknowledgements

This project has received funding from the European Research Council (ERC) under the European Union's Horizon 2020 research and innovation programme (grant agreement No 851272, ERC-StG-PE8-NanoMMES). This work was also funded by the Engineering and Physical Sciences Research Council (EPSRC, UK, EP/V047078/1), and UK Research and Innovation (UKRI) under the UK government's Horizon Europe funding (101077226; EP/Y008707/1). M.F. is grateful for funding by an UCL Engineering Impact Studentship sponsored by Semilab Co. Ltd. A.A.F. and S.G. are grateful for funding by an EPSRC New Investigator Award (EP/R035105/1).

Conflict of Interest

The authors declare no conflict of interest.

Data Availability Statement

The data that support the findings of this study are presented in the paper and Supporting Information and available from the corresponding authors upon reasonable request.

Keywords: Energy storage · Zinc metal batteries · Ion-selective membranes · Polymers of intrinsic microporosity · Coating

[1] a) Y. Liang, Y. Yao, *Nat. Rev. Mater.* **2023**, *8*(2), 109; b) Y. Zhu, Y. Cui, Z. Xie, Z. Zhuang, G. Huang, X. Zhang, *Nat. Chem. Rev.* **2022**, *6*(7), 505.

[2] a) P. Xue, C. Guo, L. Li, H. Li, D. Luo, L. Tan, Z. Chen, *Adv. Mater.* **2022**, *34*(14), 2110047; b) Q. Yang, L. Li, T. Hussain, D. Wang, L. Hui, Y. Guo, G. Liang, X. Li, Z. Chen, Z. Huang, *Angew. Chem. Int. Ed.* **2022**, *134*(6), e202112304; c) F. Wang, O. Borodin, T. Gao, X. Fan, W. Sun, F. Han, A. Faraone, J. A. Dura, K. Xu, C. Wang, *Nat. Mater.* **2018**, *17*(6), 543; d) H. Pan, Y. Shao, P. Yan, Y. Cheng, K. S. Han, Z. Nie, C. Wang, J. Yang, X. Li, P. Bhattacharya, *Nat. Energy* **2016**, *1*(5), 1; e) X. Zeng, K. Xie, S. Liu, S. Zhang, J. Hao, J. Liu, W. K. Pang, J. Liu, P. Rao, Q. Wang, *Energy Environ. Sci.* **2021**, *14*(11), 5947.

[3] a) H. Jiang, L. Tang, Y. Fu, S. Wang, S. K. Sandstrom, A. M. Scida, G. Li, D. Hoang, J. J. Hong, N.-C. Chiu, *Nat. Sust.* **2023**, *6*(7), 806; b) L. Hong, X. Wu, L. Wang, M. Zhong, P. Zhang, L. Jiang, W. Huang, Y. Wang, K. Wang, J. Chen, *ACS Nano* **2022**, *16*(4), 6906; c) D. Kundu, B. D. Adams, V. Duffort, S. H. Vajargah, L. F. Nazar, *Nat. Energy* **2016**, *1*(10), 1; d) J. F. Parker, C. N. Chervin, E. S. Nelson, D. R. Rolison, J. W. Long, *Energy Environ. Sci.* **2014**, *7*(3), 1117.

[4] a) J. Zhu, Z. Tie, S. Bi, Z. Niu, *Angew. Chem. Int. Ed.* **2024**, e202403712; b) X. Zhou, B. Wen, Y. Cai, X. Chen, L. Li, Q. Zhao, S. Chou, F. Li, *Angew. Chem. Int. Ed.* **2024**, e202402342; c) S. Chen, Y. Xia, R. Zeng, Z. Luo, X. Wu, X. Hu, J. Lu, E. Gazit, H. Pan, Z. Hong, *Sci. Adv.* **2024**, *10*(10), eadn2265.

[5] a) Z. Zhao, J. Zhao, Z. Hu, J. Li, J. Li, Y. Zhang, C. Wang, G. Cui, *Energy Environ. Sci.* **2019**, *12*(6), 1938; b) F. Porter, *Corrosion and electrochemistry of zinc*, Taylor & Francis **1997**.

[6] a) C. Li, R. Kingsbury, L. Zhou, A. Shyamsunder, K. A. Persson, L. F. Nazar, *ACS Energy Lett.* **2022**, *7*(1), 533; b) S. Liu, J. Vongsvivut, Y. Wang, R. Zhang, F. Yang, S. Zhang, K. Davey, J. Mao, Z. Guo, *Angew. Chem. Int. Ed.* **2023**, *62*(4), e202215600.

[7] H. Li, W. Jia, P. Chen, L. Wang, X. Yan, Y.-Y. Yang, *Appl. Surf. Sci.* **2023**, *607*, 155111.

[8] a) Y. Li, Z. Wang, Y. Cai, M. E. Pam, Y. Yang, D. Zhang, Y. Wang, S. Huang, *Energy Environ. Mater.* **2022**, *5*(3), 823; b) Y. Zong, H. He, Y. Wang, M. Wu, X. Ren, Z. Bai, N. Wang, X. Ning, S. X. Dou, *Adv. Energy Mater.* **2023**, *13*(20), 2300403.

[9] a) Y. Liang, Y. Wang, H. Mi, L. Sun, D. Ma, H. Li, C. He, P. Zhang, *Chem. Eng. J.* **2021**, *425*, 131862; b) H. Qiu, X. Du, J. Zhao, Y. Wang, J. Ju, Z. Chen, Z. Hu, D. Yan, X. Zhou, G. Cui, *Nat. Commun.* **2019**, *10*(1), 5374.

[10] S. Bhoyate, S. Mhin, J.-e. Jeon, K. Park, J. Kim, W. Choi, *ACS Appl. Mater. Interfaces* **2020**, *12*(24), 27249.

[11] a) S. Tian, L. Zhou, W. He, Y. Tian, Y. Zhou, S. Wu, R. Jian, K. J. Balkus, T. Luo, G. Xiong, *Chem. Eng. J.* **2023**, *462*, 142276; b) P. Tangthuam, W. Kao-ian, J. Sangsawang, C. Rojviriya, P. Chirawatkul, J. Kasemchainan, F. Mahlendorf, M. T. Nguyen, T. Yonezawa, S. Kheawhom, *Mater. Sci. Energy Technol.* **2023**, *6*, 417; c) J. Hao, X. Li, S. Zhang, F. Yang, X. Zeng, S. Zhang, G. Bo, C. Wang, Z. Guo, *Adv. Funct. Mater.* **2020**, *30*(30), 2001263.

[12] a) A. Wang, W. Zhou, A. Huang, M. Chen, J. Chen, Q. Tian, J. Xu, *J. Colloid Interface Sci.* **2020**, *577*, 256; b) J. Wang, J. G. Wang, H. Liu, Z. You, Z. Li, F. Kang, B. Wei, *Adv. Funct. Mater.* **2021**, *31*(7), 2007397.

[13] Y. Zhang, X. Li, L. Fan, Y. Shuai, N. Zhang, *Cell Rep. Phys. Sci.* **2022**, *3*(4).

[14] a) M. Liu, L. Yang, H. Liu, A. Amine, Q. Zhao, Y. Song, J. Yang, K. Wang, F. Pan, *ACS Appl. Mater. Interfaces* **2019**, *11*(35), 32046; b) L. Lei, J. Dong, S. Ke, S. Wu, S. Yuan, *Inorg. Chem. Front.* **2023**; c) V. Aupama, W. Kao-Ian, J. Sangsawang, G. Mohan, S. Wannapaiboon, A. A. Mohamad, P. Pattananuwat, C. Sriprachuabwong, W.-R. Liu, S. Kheawhom, *Nanoscale* **2023**, *15*(20), 9003.

[15] R. Tan, A. Wang, R. Malpass-Evans, R. Williams, E. W. Zhao, T. Liu, C. Ye, X. Zhou, B. P. Darwich, Z. Fan, *Nat. Mater.* **2020**, *19*(2), 195.

[16] a) C. Ye, R. Tan, A. Wang, J. Chen, B. Comesaña Gándara, C. Breakwell, A. Alvarez-Fernandez, Z. Fan, J. Weng, C. G. Bezzu, *Angew. Chem. Int. Ed.* **2022**, *134*(38), e202207580; b) C. Ye, A. Wang, C. Breakwell, R. Tan, C. Grazia Bezzu, E. Hunter-Sellars, D. R. Williams, N. P. Brandon, P. A. Klusener, A. R. Kucernak, *Nat. Commun.* **2022**, *13*(1), 3184; c) A. Wang, R. Tan, D. Liu, J. Lu, X. Wei, A. Alvarez-Fernandez, C. Ye, C. Breakwell, S. Guldin, A. R. Kucernak, *Adv. Mater.* **2023**, *35*(12), 2210098.

[17] M. J. Baran, M. E. Carrington, S. Sahu, A. Baskin, J. Song, M. A. Baird, K. S. Han, K. T. Mueller, S. J. Teat, S. M. Meckler, *Nature* **2021**, *592*(7853), 225.

[18] R. Tan, A. Wang, C. Ye, J. Li, D. Liu, B. P. Darwich, L. Petit, Z. Fan, T. Wong, A. Alvarez-Fernandez, *Adv. Sci.* **2023**, 2206888.
[19] L. Wang, R. Malpass-Evans, M. Carta, N. B. McKeown, F. Marken, *J. Solid State Electrochem.* **2020**, *24*, 2797.
[20] A. Herescu, J. S. Allen, *J. Power Sources* **2012**, *216*, 337.
[21] Q. Dai, F. Xing, X. Liu, D. Shi, C. Deng, Z. Zhao, X. Li, *Energy Environ. Sci.* **2022**, *15*(4), 1594.
[22] E. Purser, R. Stokes, *J. Am. Chem. Soc.* **1951**, *73*(12), 5650.
[23] a) Z. Yuan, Y. Duan, H. Zhang, X. Li, H. Zhang, I. Vankelecom, *Energy Environ. Sci.* **2016**, *9*(2), 441; b) P. Xiong, S. Peng, L. Zhang, A. Li, Y. Chen, S. Xiao, Q. He, G. Yu, *Chem* **2023**, *9*(3), 592; c) W. Lu, X. Li, *Acc. Mater. Res.* **2023**, *4*(8), 681.
[24] J. Ren, C. Li, P. Li, S. Liu, L. Wang, *Chem. Eng. J.* **2023**, *462*, 142270.
[25] a) X. Shi, J. Xie, J. Wang, S. Xie, Z. Yang, X. Lu, *Nat. Commun.* **2024**, *15*(1), 302; b) H. Yang, Y. Qiao, Z. Chang, H. Deng, X. Zhu, R. Zhu, Z. Xiong, P. He, H. Zhou, *Adv. Mater.* **2021**, *33*(38), 2102415.
[26] M. Wahlqvist, A. Shchukarev, *J. Electron Spectrosc. Relat. Phenom.* **2007**, *156*, 310.
[27] a) Y. Zhao, M. Li, Z. Yuan, X. Li, H. Zhang, I. F. Vankelecom, *Adv. Funct. Mater.* **2016**, *26*(2), 210; b) H. Zhang, H. Zhang, F. Zhang, X. Li, Y. Li, I. Vankelecom, *Energy Environ. Sci.* **2013**, *6*(3), 776.
[28] P. He, M. Yan, G. Zhang, R. Sun, L. Chen, Q. An, L. Mai, *Adv. Energy Mater.* **2017**, *7*(11).

Manuscript received: May 16, 2024
Accepted manuscript online: August 28, 2024
Version of record online: November 2, 2024